Falcon Telescope Network and USAFA 1-Meter Telescope Systems Limiting Magnitude Research

Timothy W. Giblin
i2 Strategic Services LLC
Cadet Chia-Hsiang Shen, Benjamin Roth, Cadet Luke King
Department of Physics and Meteorology, U.S. Air Force Academy
David M. Strong
Strong EO Imaging, Inc.
Francis K. Chun
Department of Physics and Meteorology, U.S. Air Force Academy

Abstract

We conduct a study of the limiting magnitude of the United States Air Force Academy (USAFA) suite of fourteen ground-based telescopes: the Falcon Telescope Network (FTN), and the USAFA 1-meter (USAFA-1m) telescope. This network of telescopes enables extended time-domain optical observations from multiple locations around the globe. The limiting magnitude characterizes the brightness of the faintest object detected in an image for a given signal-to-noise ratio (SNR). This information is critical to determine the system's capability to support specific astronomical and space domain awareness (SDA) research objectives. To determine the limiting magnitude, we observed multiple Landolt standard star fields close to the zenith through BVR filters with a series of exposure times. Science images were produced by applying standard image reduction techniques. Sources were extracted from each image using the DAOFIND algorithm. Instrumental magnitudes were calculated via aperture photometry and calibrated using the known Landolt standard stars in the field. The apparent limiting magnitudes for the USAFA 1-m telescope were determined as follows: $B = 18.6 \pm 0.10, V = 18.4 \pm 0.10, R = 18.2 \pm 0.10$, at a SNR $= 5$ for an exposure time of 30 seconds. A stacked image with an effective exposure time of 300 seconds $(10 \times 30s)$ produced a limiting magnitude of $R = 19.4 \pm 0.10$. Limiting magnitude analysis for the 0.5-m Falcon telescope is in progress at the time of this writing. The determination of the limiting magnitudes of the USAFA-1m and FTN telescopes will maximize research productivity and operations at USAFA.

1. INTRODUCTION

The limiting magnitude characterizes the apparent brightness of the faintest object(s) in an astronomical image for a user-specified statistical significance. Knowledge of the limiting magnitude of the US Air Force Academy's (USAFA) telescopes is essential to assess their capability to support specific astronomical and space domain awareness (SDA) research objectives, as well as support collaborative observation requests from other government agencies and civilian institutions. The limiting magnitude can be determined by performing aperture photometry on all sources extracted from observations of standard star fields (e.g. Landolt) down to a user-defined signal-to-noise threshold, examining their frequency distribution, and identifying the corresponding magnitude for a given photometric uncertainty.

The utility of the limiting magnitude allows an observer to pinpoint an optimum observing cadence for transient astronomical sources such as Gamma-Ray Bursts (GRBs) and Gravitational Wave (GW) sources whose optical flux is known to decay as a function of time [1]. In general, if the apparent brightness of a research target is known a-priori to fall below the telescope's limiting magnitude, the observation should not be attempted unless significant variability in source brightness is anticipated. In the realm of SDA, cislunar and/or deep space spacecraft can be a challenge due to their variable brightness and proximity to the Moon. The determination of the limiting magnitudes of the USAFA-1m and the Falcon 0.5-meter (FTN-0.5m) telescopes will therefore maximize research productivity

and operations at USAFA. In this paper, we present results from a limiting magnitude study of the USAFA-1m, USAFA-0.4m (now decommissioned), and Falcon-0.5m telescopes. The following sections describe the instrumentation, observations, and methodology applied to determine the limiting magnitudes. The final section presents our results and discusses future research capabilities.

Fig. 1a USAFA1-m

Fig. 1b FTN 0.5-m

Fig. 1c USAFA-0.4m

2. INSTRUMENTATION

The USAFA observatory houses a 1-meter $f/6$ ASA Ritchey–Chrétien telescope system with a direct drive fork equatorial mount (Fig. 1a). Although the system was installed in late 2019, progress toward commissioning the telescope was slowed due to the pandemic and the system did not became fully operational until early 2022. The USAFA-1m is equipped with a large format (9216 × 9232) 1110 Series Spectral Instruments E2V CCD290-99-1-F24 multi-sector CCD camera, Kron-Cousin UBVRI filters, four polarization filters ($0°, 90°, 45°, 135°$), and two transmission grating filters (200 l/mm and 720 l/mm). The CCD pixel size of 10 μm and primary focal length of 6000 mm give a plate scale of $0.34"$/pixel, resulting in a $52' \times 52'$ field of view (FoV) (nearly one square degree). The CCD is maintained at an approximately constant temperature of $-100°$C via a cryo-cooling system, resulting in minimal thermal noise.

USAFA's Falcon Telescope Network (FTN) is a global network of twelve $f/8$ Ritchey–Chrétien 0.5-meter RC-500 OS telescopes strategically positioned over a wide range of longitudes that include Pennsylvania, Australia, Chile, Germany, and multiple sites in Colorado (Fig. 1b) [2]. The purpose of the FTN is to support cadet space research and education at USAFA in the areas of SDA and astronomy. For multi-color digital imaging capability, the FTN telescopes are equipped with an Andor F47 1024 × 1024 CCD camera ($11' \times 11'$ FoV), BVR Johnson-Cousin filters, Sloan broad-band filters, and a 200 l/mm transmission grating filter. During the summer of 2023, a Falcon-0.5m was installed at the USAFA observatory to replace the decommissioned USAFA-0.4m. Commissioning of the AFA Falcon-0.5m is currently in progress.

The USAFA DFM 0.4-meter $f/8.2$ Ritchey–Chrétien equatorial mount telescope was decommissioned in late spring 2023, however it was utilized previously as part of this study (Fig. 1c). The USAFA-0.4m was equipped with an Andor U47 CCD imager (1024 × 1024), BVR Johnson-Cousins filters, a set of polarization filters, and a 200 l/mm transmission grating filter, and a $13' \times 13'$ FoV. We mention here the USAFA-0.4m technical specifications because data collections were performed in parallel with the USAFA-1m to corroborate limiting magnitude results.

3. OBSERVATIONS & METHODOLOGY

A limiting magnitude study was previously conducted on the USAFA-0.4m during the Spring of 2022 as part of a senior research capstone by observing multiple Landolt Standard Fields (SA98 SF1, SA98 SF2, and SA26) [3]. A limiting magnitude of $R = 16.1$ was determined for a signal-to-noise ratio (SNR) threshold of 10 and an exposure time of 250 seconds. This result serves as a reasonable quantitative comparison for the USAFA 1-m and Falcon 0.5-m, since, to first order, the limiting magnitude depends on the diameter of the primary. We expect a difference of $\sim 2.5 \log(D_1/D_2)^2$, where D_i represents the diameter of the primary mirrors. Comparing the USAFA-1m and the USAFA-0.4m, we anticipate the USAFA-1m limiting magnitude to be fainter by a value of ~1.99.

To determine the telescope's limiting magnitude *experimentally*, we followed the work of Davis & Giblin [4], Marsh et al. [5], and Finley et al. [3] and conducted a series of observations of Landolt Standard Fields [6, 7, 8] positioned in proximity to local zenith to ensure an air mass close to unity ($\chi \sim 1$). Observations are summarized in Table 1.

TABLE I. Landolt Field Observations

Field	α(J2000)	δ(J2000)	Obs Date	Telescope	Filters	Exposures
SA 26	$6^h\ 43^m\ 50.14^s$	+44° 38' 14.8"	2023-02-02 2023-02-10	USAFA-1m USAFA-0.4m	B, V, R	$10 \times 10s$ $10 \times 20s$ $10 \times 30s$
GD 64	$4^h\ 57^m\ 18.51^s$	+41° 55' 10.1"	2023-02-02	USAFA-1m	B, V, R	$10 \times 10s$ $10 \times 20s$ $10 \times 30s$
GD 61	$4^h\ 38^m\ 39.37^s$	+41° 10' 16.4"	2023-02-10	USAFA-1m	B, V, R	$10 \times 10s$ $10 \times 20s$ $10 \times 30s$
GD 363	$17\ 38^m\ 35.04^s$	+41° 53' 58.2"	2023-06-08 2023-08-04	FTN-Colorado Mesa University	B, V, R	$10 \times 10s$ $10 \times 20s$ $10 \times 30s$

Noise correction of all Landolt field image data was performed using standard image reduction techniques (bias, thermal, and flat-field corrections) through a USAFA Python image reduction pipeline. Ten bias frames were taken each night, and ten dark frames were taken at exposure times identical to the science images for the purpose of generating master bias and dark frames, respectively. Master flat field frames were generated by median filtering a series of five sky flats taken near the zenith at dusk for each filter. Spurious pixels were replaced with the median level of the background. For the USAFA-1m images, the final science images were trimmed from their native spatial dimension of 9216×9232 down to 6017×6017 to eliminate multiple edge effects of the multi-sector CCD. Fig. 2 shows an example of a raw image of Landolt Field GD 61 taken with the USAFA-1m and the associated reduced science image. Image data taken on 20230202 proved to be of degraded quality due to significant moonglow that resulted in a substantial gradient in the background level across the images, and therefore were not used in this study.

Automated source extraction processing was performed on each reduced Landolt science image (native exposures + stacked images) using the DAOFIND source extraction algorithm within the AstroPy Photutils package [9, 10]. The DAOFIND algorithm performs an iterative background clipping algorithm to estimate the background then scans the image for sources with the given point spread function (PSF) above a user-defined threshold. A full description can be found in Stetson [9]. The full-width half-maximum (FWHM) of the image PSF was determined for each image prior to executing the source extraction pipeline using standard radial profile fitting via Mira Pro for a sample of 10-15 stars of varying brightness across each image. The mean FWHM and user-specified detection threshold values served as the primary inputs to the DAOFIND algorithm.

Standard aperture photometry was performed using the AstroPy Photutils package in our automated source extraction pipeline on the source list identified by DAOFIND. An aperture radius of $1.5 \times$ FWHM was adopted as the optimum radius based on a curve of growth [3, 11]. An inner sky annulus radius of $1.5 \times$ FWHM and an outer radius of $2.1 \times$ FWHM was adopted to normalize the annulus area to the aperture area. The instrumental magnitudes for each

extracted source were calculated by normalizing the source aperture flux by the integration time and then calibrated via standard differential photometry using between 3 and 10 Landolt standard stars visible in each image. Calibration constants were calculated for each image and instrumental magnitudes were calibrated to the standard system.

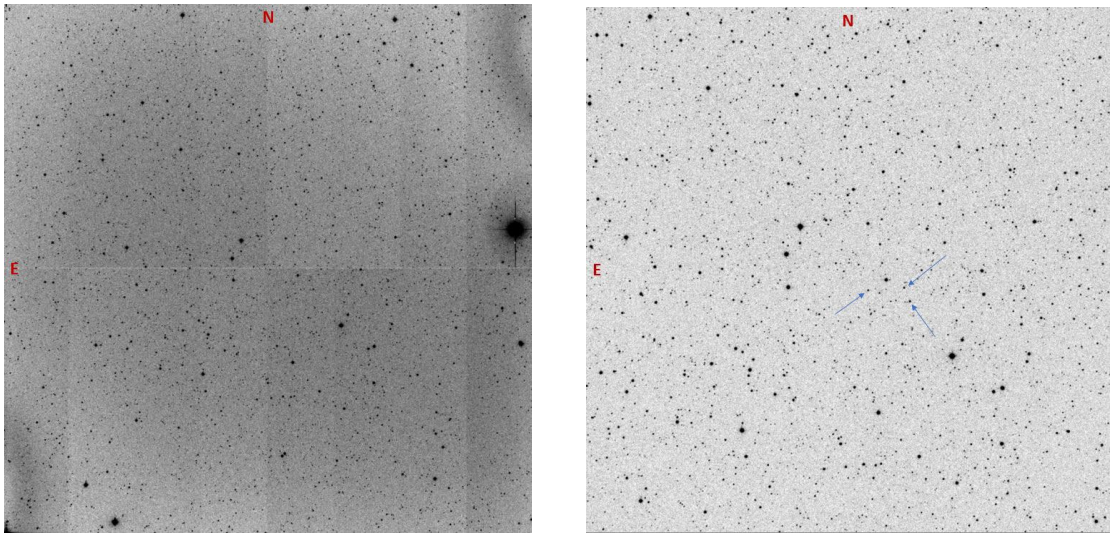

Fig 2. Raw image of Landolt Field GD 61 (*left panel*) and reduced image (*right panel*). The spatial sensitivity of the E2V CCD individual sectors are clearly visible in the raw image. The three Landolt standards are identified in the reduced image with blue arrows.

Standard error propagation was implemented in the source extraction pipeline to determine the precise photometric uncertainty for each extracted source. The uncertainty in the extracted source's apparent magnitude is given by

$$\delta m \cong \frac{1.0857\sigma_F}{F},$$

where F is the source flux within the aperture, and σ_F, the uncertainty of the source flux within the aperture (adopted from the CCD equation), is given by

$$\sigma_F = \sqrt{\frac{F}{G} + N_P\sigma_{sky}^2 + \frac{{N_P}^2\sigma_{sky}^2}{N_B}}$$

The first term under the radical represents the uncertainty in the source flux in the aperture (Poissonian), where G is the gain of the CCD. The second term represents the uncertainty in the sky noise within the aperture, where N_p is the number of pixels within the aperture and σ_{sky}^2 in the variance in the sky background. The third term represents the mean uncertainty in the sky background, where N_B is the total number of pixels used to estimate the sky background level [11].

4. ANALYSIS & RESULTS

With a comprehensive photometrically calibrated table of all detected source magnitudes down to a user-defined SNR threshold for a given science image, we were able to examine the frequency distribution of the apparent magnitude of all sources in the image, as well the performance curve by plotting apparent magnitude, m, on the ordinate and the magnitude uncertainty, δm, on the abscissa. The former provides an indication of the completeness

limit of the sources sampled, and the latter allows one to define a limiting magnitude down to a desired photometric uncertainty. In the following subsections, we address the results for each telescope system.

4.1 USAFA-1m

Skies were clear and transparent on both nights of 20230802 and 20230810. However, data taken on 20230802 were less than ideal due to a waxing crescent moon rising in the east at the time of observations, causing a prominent gradient in the sky background in all images. Since moonrise was much later on 20230810, these data are of higher quality and therefore utilized in this study to determine the limiting magnitude.

To examine the consistency in the extracted source counts in each image for a given filter and exposure time, we ran the source extraction pipeline for an SNR threshold of 5 on three different 30 second exposure images in each filter and performed a comparison (Table II). For both Landolt fields, we see that $N_R > N_V > B_B$, where N is the number of extracted sources. For any given 30 second exposure in a particular filter, we do not expect to obtain precisely the same number of extracted sources, but rather some variation likely attributable to subtle changes in the sky background between exposures as well as variations in the detector noise.

Table II. USAFA-1m 30 second exposure source count statistics for Landolt Fields SA 26 and GD 61.

	B	**V**	**R**
SA 26 – 0001	861	937	1456
SA 26 – 0002	827	987	1324
SA 26 – 0003	856	1068	1268
	$\bar{N}_B = 848 \pm 18$	$\bar{N}_V = 997 \pm 66$	$\bar{N}_R = 1349 \pm 97$
GD 61 – 0001	2029	3544	3730
GD 61 – 0002	1836	3474	3885
GD 61 – 0003	1941	3101	4085
	$\bar{N}_B = 1935 \pm 97$	$\bar{N}_V = 3373 \pm 238$	$\bar{N}_R = 3900 \pm 177$

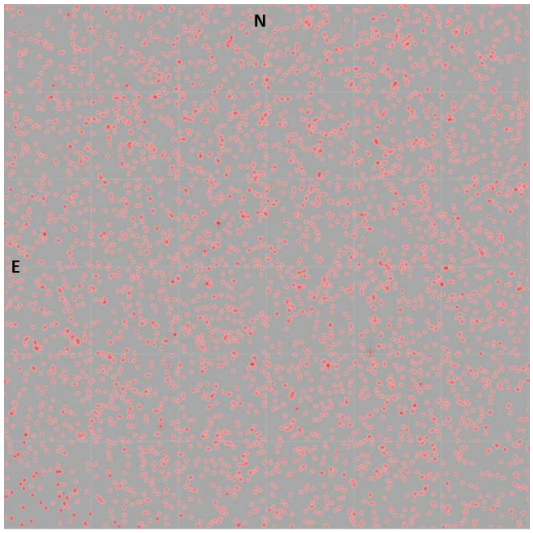

Fig 3. Source extraction results on the R-band 30 second reduced image for Landolt field GD 61. Extracted sources are spatially marked with a small red circle centered on centroid solution from DAOFIND. A total of 4085 sources were identified in the image. Image orientation is N-up, E-left.

A separate USAFA Python pipeline was constructed to align and stack images using Astroalign [12]. The additional 10 and 20 second exposures allowed the creation of a series of co-aligned and stacked images with effective exposure times greater than 30 seconds, up to and including 300 seconds. Fig. 4 illustrates the number of extracted sources as a function of exposure time for Landolt field GD 61. At shorter exposure times the behavior appears linear, however as the exposure time increases, the non-linearity behavior is apparent as the number of sources begins to bend over near ~120 seconds owing to the finite sensitivity of the system.

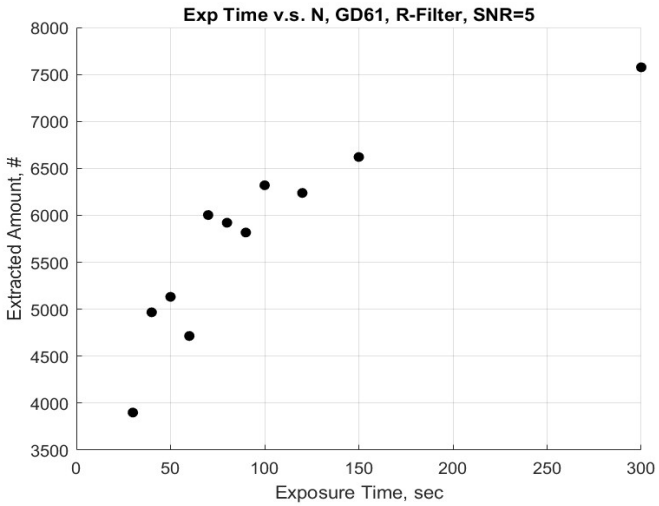

Fig 4. Source extraction results as a function of exposure time for Landolt field GD 61, R-band, with a threshold SNR value of 5. Effective exposure times greater than 30 seconds were obtained by aligning and stacking images of shorter exposure times (e.g. $7 \times 10\text{s} = 70\text{s}$).

Insight into the limiting magnitude of the system is gained by examining the frequency distribution of source magnitudes and the performance curve (m vs. δm) for a given exposure. Here we focused on the 30 second exposures images because we expect more fainter sources in the 30 second image than shorter exposure images. The histogram and performance curve for the 30 second R-band images of SA 26 are shown in Fig. 5. The histogram (left panel) suggests a completeness limit down to 18$^{\text{th}}$ magnitude. Sources fainter than 18$^{\text{th}}$ magnitude are clearly under-sampled and near the detection limit. Although some of these sources may appear to be present in the image upon visual inspection, they did not meet the source extraction criteria. The performance curve of m vs. δm (right panel) exhibits a quasi-asymptotic behavior that demonstrates that same decrease in sensitivity down to 18$^{\text{th}}$ magnitude. This curve allows us to quote a limiting magnitude for a given photometric accuracy. For 10% photometry, we extract a limiting magnitude value $m_l = 18.2$ from the performance curve. For 5% photometry, we can quote $m_l = 17.4$ from the performance curve. Note that (extracted) sources beyond the completeness limit (i.e., tail end of the histogram at faint magnitudes) are still present in the performance curve, however their magnitudes may increase only marginally while their corresponding photometric uncertainties dramatically increase. The utility of the performance curve not only sheds light on our magnitude limit of the faintest sources in the image, but also has critical application for specific science objectives. For example, exoplanet transit observations often require milli-magnitude precision to identify the dip in the light curve of the parent star. The R-band performance curve suggests that under optimum seeing conditions, the parent star limiting magnitude is approximately 14.4. Observing a 16$^{\text{th}}$ magnitude parent start for an exoplanet transit would therefore not provide the required photometric accuracy to detect the planetary occultation of the planet star.

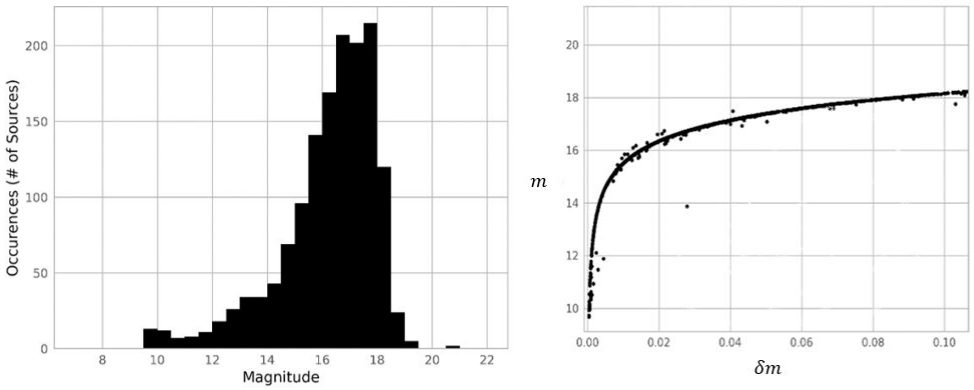

Fig 5. Magnitude histogram (*left panel*) and performance curve (*right panel*) for all detected sources in the 30 second R-band image of Landolt field SA 26.

Table III summarizes the limiting magnitude results for the 30 second images for Landolt fields SA 26 & GD 61. These results are consistent (within two sigma) between different Landolt fields on the sky under highly similar observing conditions with only minor variations between broadband filters.

Tabel III. Limiting Magnitude (m_l) results for each broadband filter quoted at 5% and 10% photometry.

	Landolt Field SA 26		**Landolt Field GD 61**	
	$m_l\ (\delta m = 0.05)$	$m_l\ (\delta m = 0.10)$	$m_l\ (\delta m = 0.05)$	$m_l\ (\delta m = 0.10)$
B	17.9	18.6	17.7	18.5
V	17.5	18.1	17.7	18.4
R	17.4	18.2	17.3	18.1

Does increasing the exposure time increase our limiting magnitude of the system? Since we have co-aligned and stacked images with effective exposure times beyond 30 seconds, we were able to run the limiting magnitude analysis on these data to examine the behavior of the limiting magnitude as a function of exposure time. We performed this exercise for the R-band with an SNR threshold of 5 for Landolt field GD 61.

From the $10 \times 10\text{s}, 10 \times 20\text{s}, \text{and } 10 \times 30\text{s}$ exposures, we constructed effective exposure times by stacking equal exposure images. Effective exposure times greater than 30 s were obtained by aligning and stacking images of shorter exposure times (e.g. $7 \times 10\text{s} = 70\text{s}$). Fig. 6 shows a plot of the limiting magnitude as a function of exposure time. Note that these data are sampled in 10 second intervals up to 100 seconds, and unevenly sampled beyond that time due to the limited exposure times available in the data. Similar to the source extraction counts in Fig. 4, we observe an approximately linear relationship followed by a turnover that begins near ~100 seconds, attributable to the finite sensitivity of the system. Exposing beyond ~2 minutes offers little in return. For example, for 10% photometry one can double the exposure time of 150 seconds to 300 seconds and only gain $\Delta m_l \approx 0.4$. A nearly identical difference between the 150 and 300 second effective exposures is also observed for the 5% photometry.

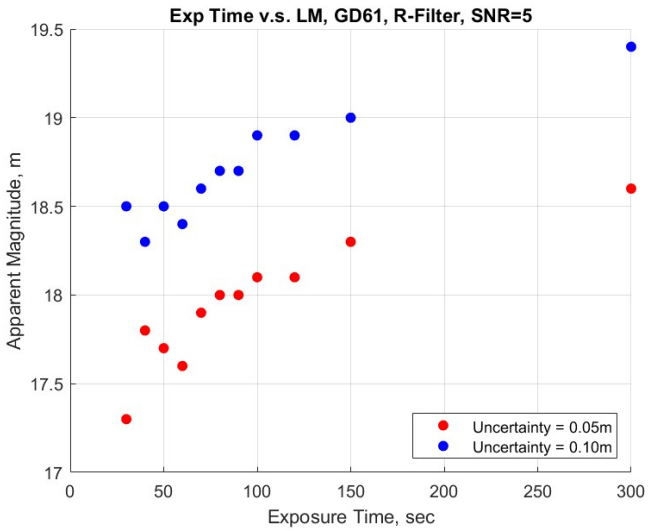

Fig 6. R-band limiting magnitude down to an SNR threshold of 5 for Landolt Field GD 61, shown as a function of time. Limiting magnitudes trends are shown for 5% (*red*) and 10% (*blue*) photometry.

4.2 USAFA-0.4m

In spite of the impending decommissioning of the USAFA-0.4m telescope at the Air Force Academy observatory, the limiting magnitude study was executed for this system primarily as a validation check for the USAFA-1m results. Contemporaneous observations of the same Landolt fields by each system effectively removes any differences in limiting magnitude due to site dependencies (since USAFA-0.4m and USAFA-1m are collocated). Since these observations were also subject to the same moonglow effects in the background on 20230202, this limiting magnitude analysis was only applied to the 20230210 data.

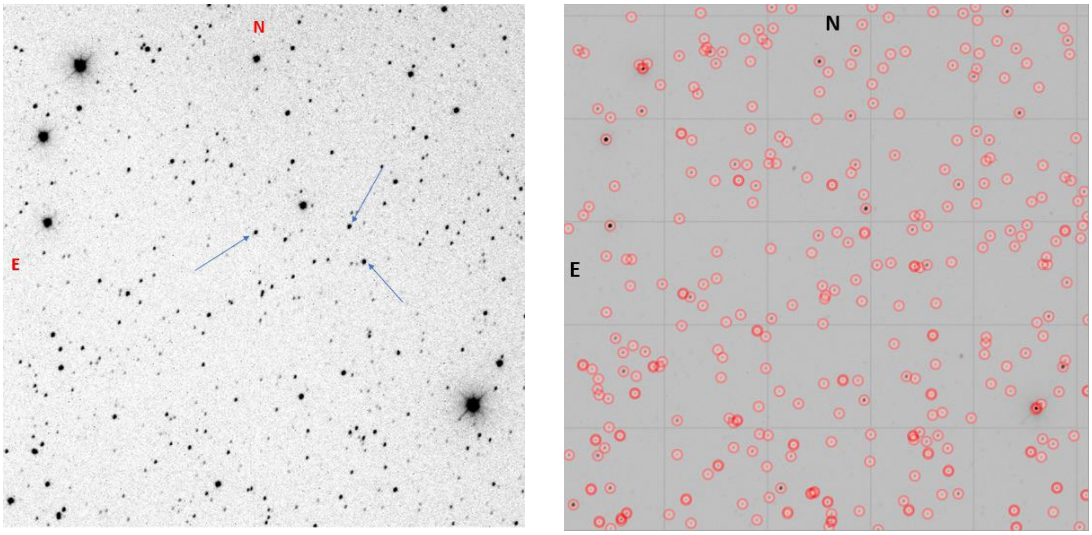

Fig. 7. Reduced 30 second R-band image of Landolt Field GD 61 (*left panel*). Landolt standards are identified by the blue arrows. A total of 331 extracted sources are spatially identified with a small red circle (*right panel*).

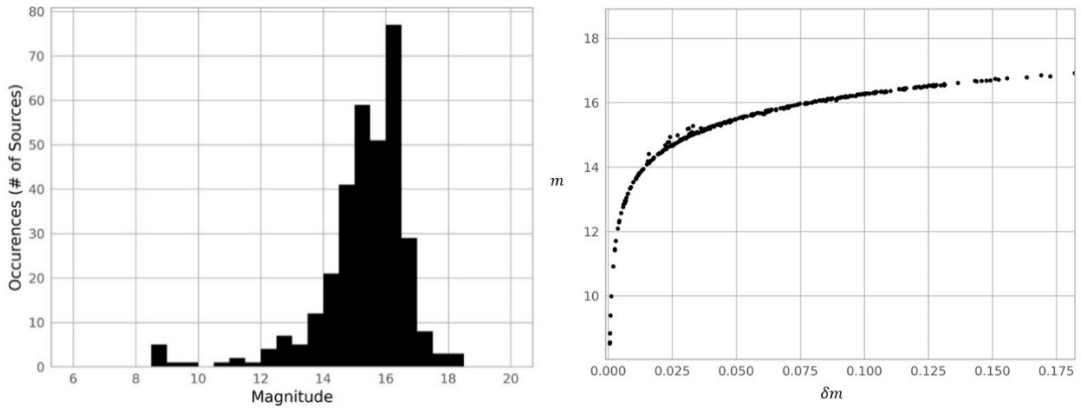

Fig. 8. Magnitude histogram (*left panel*) and performance curve (*right panel*) for all detected sources in the 30 second R-band image of Landolt field GD 61.

Fig. 7 shows the reduced 30 second R-band image of Landolt field GD 61 as well as the source extraction results for an SNR threshold of 5. The undetected sources near threshold are more easily seen in the USAFA-0.4m images due to the smaller FoV.

The USAFA-0.4m histogram shown in Fig. 8 indicates a completeness down to approximately $m \cong 16.2$. The performance curve shows a limiting magnitude $m_l = 15.4$ for 5% photometry and $m_l = 16.2$ for 10% photometry. When comparing the diameter of the primary mirror only to the USAFA-1m we expect a limiting magnitude brighter by ~1.9 magnitudes. Adding a difference of 1.9 to these values recover the USAFA-1m limiting magnitude values for a 30 second exposure in the R-band at an SNR detection threshold of 5. *The USAFA-0.4m data validates our results for the USAFA-1m.*

4.3 FTN-0.5

Due to weather and additional operational constraints, Landolt field observations were not possible for all eleven FTN nodes for this analysis. Observations on 20230608 & 20230804 were taken using the Colorado Mesa University (CMU) FTN node located in Grand Junction, CO. In spite of clear skies, data taken on 20230608 are problematic due to anomalous autoguiding issues that produced highly elongated point spread functions. Data taken on 20230804 are limited in quantity ($3 \times 30s$, R-band) due to occasional and sporadic clouds in the area. Nonetheless, we had sufficient data to at least perform a preliminary limiting magnitude estimate for the CMU Falcon telescope.

The R-band FTN-CMU images were reduced using the same pipeline with one caveat: no flat fielding was performed on the GD 363 science images. The sky flats in hand were too few in number to remove all sources via median filtering in the master flat. Various flat fielding strategies are currently being pursued by the FTN operations team. A reduced 30 second R-band FTN-CMU image of GD 363 is shown in the left panel of Fig. 9. The image is shown in color to emphasize the presence of the non-flatness in the reduced image. The right panel of Fig. 9 shows the source extraction results with an SNR threshold of 3 rather than the more conservative approach (SNR threshold = 5) taken with the USAFA-1m and the USASFA-0.4m. Upon detailed inspection of the image, the focus was determined to be less than optimum. Many sources near the detection threshold were therefore not detected. This is apparent in the magnitude frequency distribution shown in Fig. 10. This field is clearly under-sampled due to the poor focus and the unflattened image. However, we are able to gain some insight into the depth of the image from the performance curve shown in the right panel of Fig. 10. The curve turns over, as expected, and demonstrates similar behavior as the USAFA-0.4m. For 5% photometry, we find $m_l \cong 15.3$ and for 10% photometry we find $m_l \cong 16.0$ from a logarithmic interpolation. Naturally we would expect these FTN-0.5m numbers to be slightly

deeper than those derived for the USAFA-0.4m. However, the out of focus image produced flatter stellar PSFs resulting in a decrease in flux near the central peak of the PSF. A considerable fraction of that flux is lost in the broad wings of the PSF and even contributes to an increase in the sky background in the annulus. Manual steps therefore need to be taken to refocus the CMU Falcon and ensure that the system autoguiding is operating nominally. Once clear skies return, these observations will be repeated to verify the expected FTN-CMU limiting magnitude.

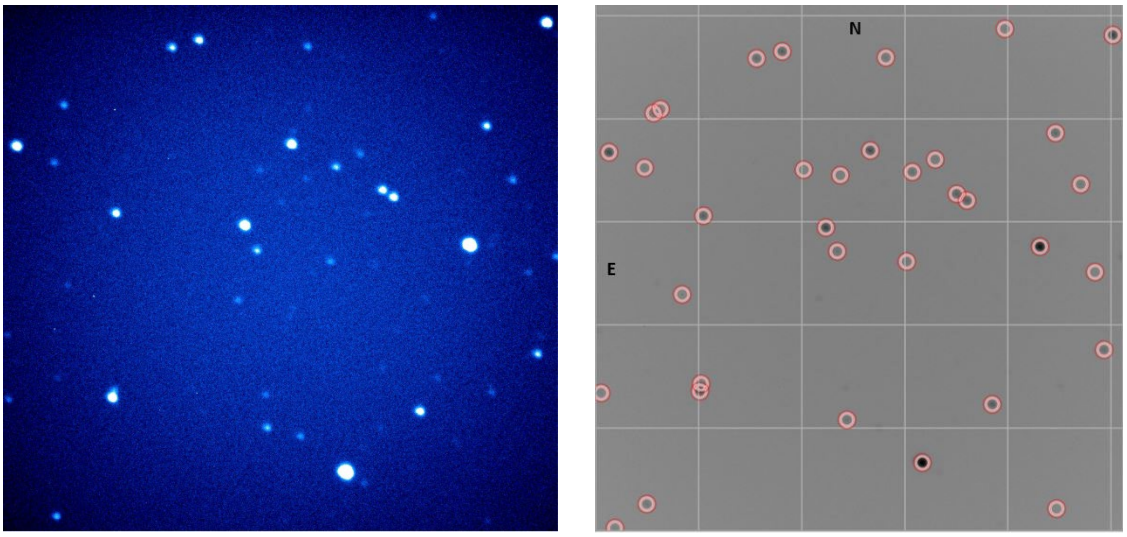

Fig. 9. Reduced FTN-CMU 30 second R-band image of GD 363 taken with the Falcon CMU telescope (*left panel*). Note the circular non-flatness centered in the image (bias and dark corrections only). Extracted sources at an SNR threshold of 3 revealed a total of 35 sources in the image (*right panel*).

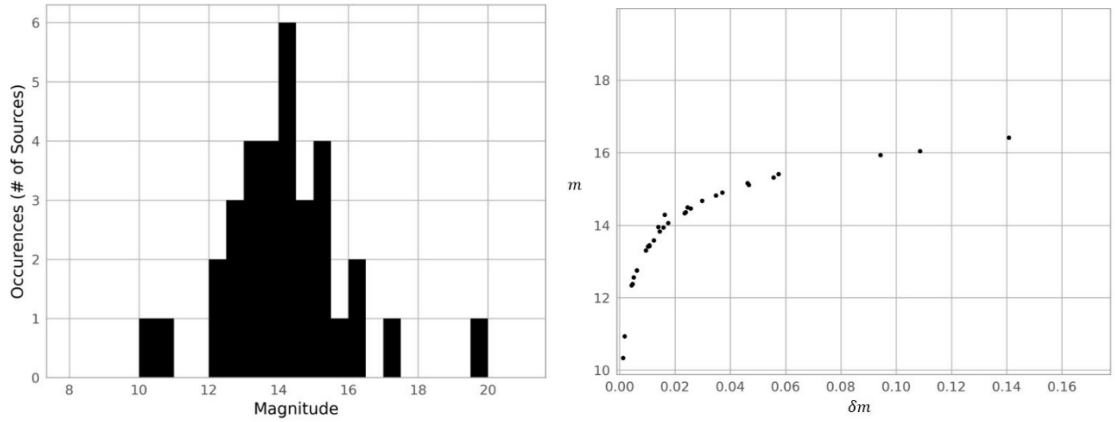

Fig. 10. Magnitude histogram (*left panel*) and performance curve (*right panel*) for all detected sources in the 30 second R-band image of Landolt field GD 363.

5. CONCLUSION

Our study of the limiting magnitude of US Air Force Academy telescope assets has provided insight into our observational capabilities as well as guidance on the optimum observing cadence to execute for various types of astronomy and SDA research projects. Our analysis demonstrates that the USAFA-1m can go as deep as 18.2 in the R-band (30 s exposure) for a photometric accuracy of 10%. Doubling the exposure time offers only marginal improvement. These results are fully corroborated by the simultaneous observations made with the USASFA-0.4m telescope. Our results will allow the USAFA-1m to perform exoplanet transit observations of parent stars down to a limit of 15th magnitude and observe the optical counterparts to high-energy transient events such as GRBs and GW sources up to ~1.5 days following the event [1]. The USAFA-1m will also enable key observations in SDA research. Most GEO spacecraft have visual magnitudes in the $\sim 11 - 14$ range. Thus the USAFA-1m should be effective in monitoring these spacecraft and any variability in their brightness, as well as smaller spacecraft in GEO that may prove to be considerably dimmer and more challenging to detect. Ground-based observations of cislunar spacecraft may prove to be more of a challenge as the spacecraft brightness decays with distance from Earth [13], however it should be noted that the apparent magnitude of several Apollo spacecraft were reported to also fall in the same 11-14th visual magnitude range [14]. We are encouraged that the deep detection capability of the USAFA-1m may allow us to continuously observe cislunar spacecraft, constrained only by position in the sky.

The limiting magnitude derived for the Falcon telescope located at Colorado Mesa University, although influenced by the adverse observations at the time, also exhibits results consistent with the USAFA-0.4m and the USAFA-1m telescopes. The FTN is currently in the process of numerous hardware upgrades. Once these upgrades, anticipated to be complete by the end of calendar year 2023, are in place, the limiting magnitude study for the full complement of Falcon telescopes in the network can be swiftly performed so that specific capabilities can be identified for each site.

Since the decommissioning of the USAFA-0.4m telescope at the USAFA observatory during early 2023, a new 0.5m Falcon telescope (the "AFA Falcon") has been installed with upgraded hardware (including PlaneWave Instruments L-500 mount). At the time of the writing of this paper, the telescope is awaiting filter-wheel and camera installation, followed by commissioning exercises. Once the AFA Falcon is fully operational, we will have the capability to survey multiple Landolt fields and perform the limiting magnitude analysis locally at the USAFA observatory. For the AFA Falcon, we would expect a limiting magnitude close to ~ 17 based on the results for the USAFA-0.4m (now decommissioned) and the USAFA-1m.

6. ACKNOWLEDGEMENTS

The US Air Force Academy Center for Space Situational Awareness (CSSAR) research team is grateful to Dr. Devin Della-Rose for instrument support for the USAFA-1m system. We are also grateful to USAF 2nd Lts and USAFA graduates Seth Finley and Madison Marsh for laying the groundwork for much of this analysis. We also want to acknowledge the support of the Air Force Office of Scientific Research. Additionally, a significant portion of this paper is the result of an independent research project during the 2023 Spring semester in the Department of Physics and Meteorology at the United States Air Force Academy.

7. PUBLIC RELEASE AND DISCLAIMER

8. REFERENCES

[1] I. Andreoni et al., Follow Up of GW170817 and its Electromagnetic Counterpart by Australian-led Observing Programs, *Publications of the Astronomical Society of Australia* (PASA), 34: 69-80, 2017.

[2] F. K. Chun et al., A new Global Array of Optical Telescopes: The Falcon Telescope Network, *Publications of the Astronomical Society of the Pacific* (PASP), 130: 095003-095024, 2018.

[3] S. Finley, D. Della-Rose, T. W. Giblin, & F. Chun, Limiting Magnitude Study of USAFA Telescopes, Senior Capstone, US Air Force Academy, 2022.

[4] K. Davis & T. W. Giblin, Detection Limit for the Apogee AP6Ep CCD on the 40 cm DFM Telescope, Senior Capstone, The College of Charleston, 2004.

[5] M. Marsh, T. W. Giblin, P. Gokuldass, B. Orange, & D. Della-Rose, A Limiting Magnitude Study of the Virgin Islands Robotic Telescope (VIRT), *Colorado Springs Undergraduate Research Forum*, 2021.

[6] A. U. Landolt, UBVRI Photometric Standard Stars in the Magnitude Range $11.5 < V < 16.0$ Around the Celestial Equator, *The Astronomical Journal*, 104: 340-491, 1992.

[7] A. U. Landolt, UBVRI Photometric Standard Stars Around the Celestial Equator: Updates and Additions, *The Astronomical Journal*, 137: 4186-4269, 2009.

[8] A. U. Landolt, UBVRI Photometric Standard Stars Around the Sky at $+50$ deg Declination, *The Astronomical Journal*, 146: 131-172, 2013.

[9] P. B. Stetson, *Publication of the Astronomical Society of the Pacific*, 99: 191-222, 1987.

[10] E. Bertin & S. Arnouts, *Astronomy & Astrophysics Supplement*, 117: 393, 1996.

[11] S. B. Howell, *Handbook of CCD Astronomy*, 2nd Ed. Cambridge University Press, 2006.

[12] M. Beroiz, J. Cabral, and B. Sanchez, Astroalign: a Python Module for Astronomical Image Registration, *Astronomy and Computing*, 32: 100384, 2020.

[13] M. J. Holzinger, C. C. Chow, and P. Garretson, A Primer on Cislunar Space, *Air Force Research Laboratory* (AFRL) distribution 1271, 2021.

[14] Observer's Page, *Sky & Telescope*, Vol. 39 No. 1, p. 127, February 1970.